Double-exposure mask synthesis using inverse lithography

Amyn Poonawala
University of California, Santa Cruz
Computer Engineering Department
Santa Cruz, California 95064
E-mail: amyn@soe.ucsc.edu

Peyman Milanfar
University of California, Santa Cruz
Electrical Engineering Department
Santa Cruz, California 95064

Abstract. Inverse lithography mask design and double-exposure lithography are two technologies that have gained a lot of attention in the recent past. Inverse lithography consists of synthesizing the input mask that leads to the desired output wafer pattern by inverting the mathematical forward model from mask to wafer. Double-exposure lithography uses two pairs of mask and exposure to print a single (desired) wafer pattern. It usually involves splitting the latter into two parts. In this work, we present some preliminary results in our unique effort to combine the previous two powerful techniques. The goal is to use the inverse imaging approach to automatically synthesize the masks required to print the desired wafer pattern employing double-exposure lithography. We employ the pixel-based mask representation, analytically calculate the gradient, and use a cyclic coordinate descent optimization algorithm to synthesize the two masks. We present results for chromeless phase-shift masks for an idealized case of a coherent imaging system ($\sigma=0$) using the Kirchhoff approximation. The results indicate that our algorithm automatically splits the target pattern into two (overlapping) parts, which are used separately during the individual exposures. Furthermore, the proposed approach is also capable of resolving the phase conflicts. The comparison with a single-exposure case indicates a superior contrast and no hot-spots. [DOI: 10.1117/1.2794767]

Subject terms: inverse lithography; double-exposure lithography; phase conflict; pattern decomposition; mask design; phase-shift masks; inverse problems; regularization.

Paper 06057RR received Aug. 10, 2006; revised manuscript received Jun. 6, 2007; accepted for publication Jul. 3, 2007; published online Oct. 19, 2007. This paper is a revision of a paper presented at the SPIE Conference on Optical Microlithography XX, Feb. 2007, San Jose, Calif. The paper presented there appears (unrefereed) in SPIE Proceedings Vol. 6520.

1 Introduction and Background

Inverse lithography (ILT) is an *image synthesis or image design*[1,2] problem, which consists of finding an image that, when used as the input to a given imaging system, results in the desired output image (to within some prescribed tolerance). ILT attempts to synthesize the mask by inverting the mathematical forward model from mask to wafer. Recent studies have shown than edge-based approaches[3] may not be very suitable for 45 nm and smaller nodes due to increase in the fragmentation, inability to generate assist bars, etc. Hence, there has recently been a revival of interest in pixel-based ILT approaches.[4–7]

In this work, we extend our earlier proposed single-exposure ILT framework[7] to double-exposure lithography (DEL) systems. Double-exposure lithography has gained a lot of importance recently and is tipped as one of the important technologies for enabling 45 nm and smaller technology nodes.[8,9] DEL uses two (same or different) masks and two (same or different) illumination settings to print the desired circuit pattern. There are many variants of DEL such as using a trim mask with alternating phase-shift masks (PSM),[10] double dipole lithography (DDL), innovative double-exposure by advanced lithography (IDEAL),[8] etc. Another technique, called double patterning lithography (DPL),[8] involves developing, etching, and coating the resist after the first exposure. Thus, the resist is totally developed twice. DPL doubles the resolution limit of the imaging system, allowing $k_1 < 0.25$. Zaidi & Brueck,[11] and Chen & Brueck[12] also proposed using multiple exposures with interferometric lithography for periodic and arbitrary 2-D patterns.

In this work, we consider DEL systems where the resist is developed only once at the end of the two exposures. All DEL systems involve some sort of pattern decomposition targeted toward the individual exposures. A typical DDL scheme proposed by Hsu et al.[9] starts by separating the target into horizontal and vertical geometries for use with Dy and Dx dipoles, respectively. The final image with the two exposures is the sum of the energies at the wafer plane. Therefore, a critical shielding/protecting step is essential to guarantee a high aerial image contrast. Thus, the vertical features are protected when the horizontal features are imaged and vica-versa. The previous steps are followed by scattering bar insertion and model-based optical proximity correction (OPC) to improve robustness and bring the contours on target.

Figure 1 is a simple example that demonstrates the effect

1537-1646/2007/$25.00 © 2007 SPIE

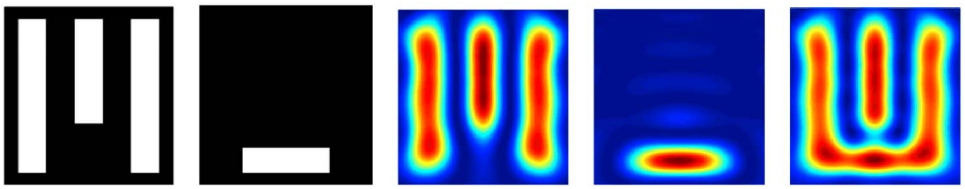

Fig. 1 Left to right: the vertical and horizontal (decomposed) target patterns, the corresponding aerial images obtained using single exposure ILT masks, and the combined aerial image.

of residual aerial image energy in DEL. Here, the target pattern was first decomposed into H and V structures (see the two patterns on the left) and the corresponding masks were synthesized. The individual aerial images are illustrated in Fig. 1 and they have a good contrast. However, we observe that the combined aerial image has an unacceptable quality at the critical junction (the gap between the horizontal and vertical features) due to the unwanted residual energy from the previous exposure. Thus, some sort of model-based pattern decomposition or shielding is essential for the success of DEL. The double-exposure inverse lithography (DEL-ILT) framework proposed in this work is an *aerial image aware* pattern decomposition. Most commonly employed techniques aim to split the (binary) target into two parts, followed by some postprocessing steps to obtain a high-contrast aerial image. However, the DEL-ILT framework is a fresh paradigm that acts by decomposing the (gray-level) aerial image into two overlapping parts. The estimated masks are simultaneously synthesized to guarantee a superior contrast of the combined aerial image without worrying about the residual energies from the previous exposure.

At the onset, we would like to highlight the goals and limitations of our study. Our work primarily focuses on exploring the feasibility and limitation of DEL-ILT solutions that provide for the aerial image contrast necessary for patterning at $k_1 < 0.35$. We employ the Kirchhoff (thin-mask) model and coherent illumination to simplify the calculations, and demonstrate the principle working of our algorithm. However, the use of the Kirchhoff approximation for forward imaging for chromeless phase lithography (CPL) (or indeed even binary) masks with sufficiently subwavelength feature sizes will lead to unacceptably large errors in mask-transmitted near-field amplitudes and phases estimation. This in turn will lead to catastropsic patterning liabilities in imaging media (resist). Therefore, accurate and computationally efficient approximation of rigorous electric-field computation needs to be found (formulated), and used for reducing the proposed algorithm to useful practices. Similarly, the framework needs to be extended to partially coherent imaging systems to account for the more practical ($\sigma > 0$) scenario. The prior considerations are currently ignored and beyond the scope of this research.

The work is organized as follows. In Sec. 2 we introduce the inverse lithography problem and discuss the forward model for DEL. We propose two algorithms for double-exposure inverse lithography, which are discussed in Sec. 3. The results are discussed in Sec. 4, and the conclusions are provided in Sec. 5.

2 Inverse Lithography and Double-Exposure Lithography Forward Model

The first step toward solving an *inverse* problem is to define a *forward* (or process) model that is a mathematical description of the given imaging system. The image formation process for a DEL system can be mathematically expressed as,

$$z(x,y) = T\{a(x,y), b(x,y)\}, \tag{1}$$

where $T\{.\}$ is the forward model that maps the input intensity functions $a(x,y)$ and $b(x,y)$ to the output intensity function $z(x,y)$. Let $z^*(x,y)$ be the desired output intensity function. The goal of double-exposure inverse lithography mask design is to estimate the input intensity functions $\hat{a}(x,y)$ and $\hat{b}(x,y)$, which give us a close approximation to the desired output $z^*(x,y)$ (see Fig. 2).

A typical lithography process consists of aerial image formation and the resist process. If the forward model $T\{.\}$ accounts for the resist effects, the output pattern $z(x,y)$ represents the resist pattern in the wafer. If $T\{.\}$ only models the imaging optics, $z(x,y)$ represents the aerial image in the wafer plane. The objective of the inverse problem in the first case is to improve the contour fidelity, and in the sec-

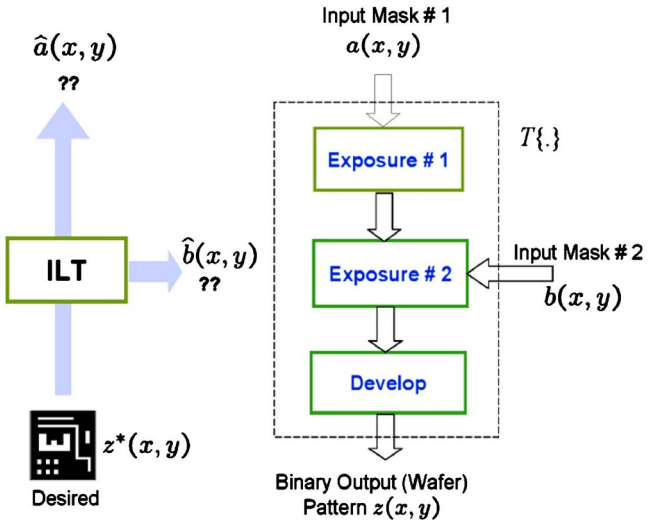

Fig. 2 Forward model and ILT for double-exposure lithography systems.

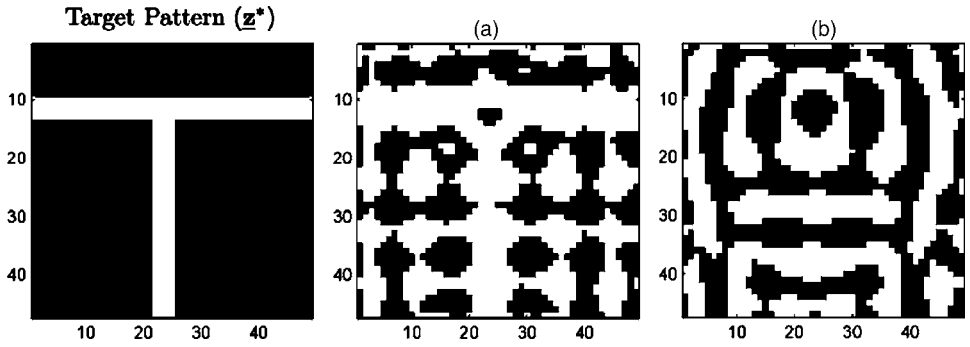

Fig. 3 The T-junction target pattern (left) and the two estimated chromeless PSM (center and right).

ond case is to improve the aerial image contrast. The current work focuses on the latter case of aerial image improvement.

The final aerial image for the given DEL system is equal to the sum of the aerial images obtained from the two individual exposures. Using the sum of coherent systems (SOCS) approximation for partially coherent imaging systems, the aerial image $\mathbf{z}$ can be modeled as,

$$\mathbf{z} = \left(\sum_{j=1}^{P_1} \gamma_j |\mathbf{H}_j \mathbf{a}|^2 \right) + \left(\sum_{j=1}^{P_2} \lambda_j |\mathbf{G}_j \mathbf{b}|^2 \right), \tag{2}$$

where $\mathbf{a}$, $\mathbf{b}$, $\mathbf{z} \in \Re^{MN \times 1}$ are obtained by sampling and lexicographic ordering of $a(x,y)$, $b(x,y)$, and $z(x,y)$, respectively, $\mathbf{H}_1, \ldots, \mathbf{H}_{P_1}$ and $\mathbf{G}_1, \ldots, \mathbf{G}_{P_2}$ are the SOCS kernels corresponding to the two exposures, and $\gamma_1, \ldots, \gamma_{P_1}$ and $\lambda_1, \ldots, \lambda_{P_2}$ respectively correspond to their singular values. Note that the previous model can account for different illumination settings for the first and second exposures (commonly seen in double dipole lithography).

In this work, as a proof of principle, we focus on the simpler case of a DEL system using a coherent imaging system ($\sigma = 0$) with the same exposure settings for both exposures. Under the previous assumptions, the forward model in Eq. (2) reduces to,

$$\mathbf{z} = |\mathbf{H}\mathbf{a}|^2 + |\mathbf{H}\mathbf{b}|^2, \tag{3}$$

where $\mathbf{H}$ is a, *jinc* function with cutoff frequency NA/λ. Alternatively, $\mathbf{H}$ can also be substituted by the optimal coherent approximation (OCA) kernel reported in Ref. 13.

The only related work (in open literature) on double-exposure mask design using inverse lithography is by Wang, et al.[14] and Pati and Kailath.[13] Their original goal was to actually solve the inverse problem for single-exposure phase-shift mask design. The mask was synthesized in the frequency domain using projection onto convex sets (POCS) iterations. The resulting mask was complex valued, having continuous phase and amplitude. Double-exposure was suggested only as a *phase quantization* technique by employing the double-exposure theorem.[14] The latter states that any image attainable using a complex-valued mask can be obtained using a suitable pair of two strong continuously varying phase-shift masks. Finally, the amplitude was quantized using half-toning. Note that they did not originally set out to design masks for double-exposure systems, and hence their framework is more restricted. It can inherently handle only coherent imaging systems, and that too with the *same* illumination settings for both exposures. Furthermore, the half-toning technique[14] tremendously increases the complexity of the masks. Finally, it is hard and not intuitive to impose simplicity and discretization constraints on the masks in the frequency domain.

In the next section, we discuss our inverse imaging approach for pixel-based DEL mask design.

3 Optimization Problem Formulation

The mask synthesis problem can be formulated as minimizing the L_2 norm of the difference between the desired pattern $\mathbf{z}^*$ and the aerial image $\mathbf{z}$ defined in Eq. (3),

$$[\hat{\mathbf{a}}, \hat{\mathbf{b}}] = \underset{\mathbf{a},\mathbf{b}}{\operatorname{argmin}} F(\mathbf{a},\mathbf{b}) = \underset{\mathbf{a},\mathbf{b}}{\operatorname{argmin}} \| \mathbf{z}^* - |\mathbf{H}\mathbf{a}|^2 - |\mathbf{H}\mathbf{b}|^2 \|_2^2. \tag{4}$$

For a chromeless phase-shift mask, the transmission values of the estimated mask pixels should be either -1 (fully transmissive with 180-deg phase shift) or $+1$ (fully transmissive with zero-deg phase shift). Therefore, the optimization problem in Eq. (4) is an integer optimization problem. It can be reduced to a continuous variable optimization problem by imposing the following $2MN$ bound constraints on the estimated variables,

$$-1 \le a_j \le -1 \quad \text{and} \quad -1 \le b_j \le 1 \text{ for } j = 1, \ldots, MN. \tag{5}$$

The prior procedure helps reduce the problem to the continuous domain, thereby enabling the usage of an analytically calculated gradient to systematically explore the solution space. The estimated masks are finally thresholded using optimum thresholds t_a and t_b to obtain the (physically realizable) two-toned masks.[15]

It is important to realize that the number of unknown parameters in double-exposure ILT is twice as many as those in a single-exposure ILT. Indeed, the inverse problem for DEL is severely ill-posed and there may be multiple pairs of eligible mask solutions. In Ref. 15, we introduced the regularization framework to overcome the earlier issue. The latter incorporates prior information about the solution to arrive at the *preferred* solution. For example, solving the problem in the continuous domain results in continuous tone masks, which are physically unrealizable. Hence, there

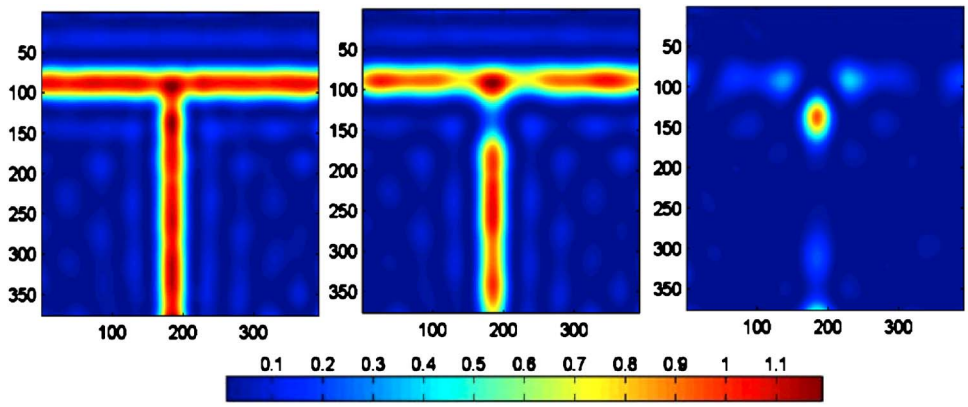

Fig. 4 The final aerial image (left) and the aerial images corresponding to the two individual exposures (center and right) for the mask patterns in Fig. 3.

is a need to control the transmission values of the estimated mask. The previous requirements can be incorporated into the optimization problem by augmenting it with suitable penalty terms, which direct the unknown parameters **a** and **b** toward the desired solution space. (A discussion on the regularization framework for inverse lithography can also be found in Refs. 7 and 16.) In our case, we employ a quadratic penalty term with zero penalty for transmission values of −1 and 1 (see Ref. 7 for more details). The discrete tone mask can then be obtained by simply thresholding the estimated masks with $t_a = t_b = 0$.

The regularization framework can also possibly be used to promote other *desirable* properties like tolerance to alignment errors, low complexity and ease of manufacturing, low mask error enhancement factor (MEEF), and good process window. In Ref. 15, we demonstrated its effectiveness to control the complexity of estimated masks (for single-exposure ILT), and are currently looking into the other potential applications. We now discuss two gradient-based algorithms for solving the bound-constrained optimization problem. These algorithms will also help to demonstrate the existence of multiple solutions.

3.1 *Method 1: Simultaneous Descent*

The first method consists of finding the gradient of the cost function defined in Eq. (4) with respect to the $2MN$ unknown parameters, and searching through the *entire* $2MN$ dimensional space using steepest descent iterations. The gradient of the cost function in Eq. (4), with respect to the parameter vectors **a** and **b**, is denoted as $\nabla_{\mathbf{a}} F(\mathbf{a},\mathbf{b})$ and $\nabla_{\mathbf{b}} F(\mathbf{a},\mathbf{b})$ where,

$$\nabla_{\mathbf{a}} F(\mathbf{a},\mathbf{b}) = -\mathbf{H}[(\mathbf{z}^* - |\mathbf{Ha}|^2 - |\mathbf{Hb}|^2) \odot (\mathbf{Ha})] \in \Re^{MN\times 1}, \tag{6}$$

$$\nabla_{\mathbf{b}} F(\mathbf{a},\mathbf{b}) = -\mathbf{H}[(\mathbf{z}^* - |\mathbf{Ha}|^2 - |\mathbf{Hb}|^2) \odot (\mathbf{Hb})] \in \Re^{MN\times 1}. \tag{7}$$

The steepest descent algorithm requires a user-defined initialization to start its iterations. However, it is interesting to note from Eqs. (6) and (7) that the gradients have the same functional form. Hence, if $\mathbf{a}^0 = \mathbf{b}^0$ (i.e., the two masks are initialized to the same value), then for all the iterations,

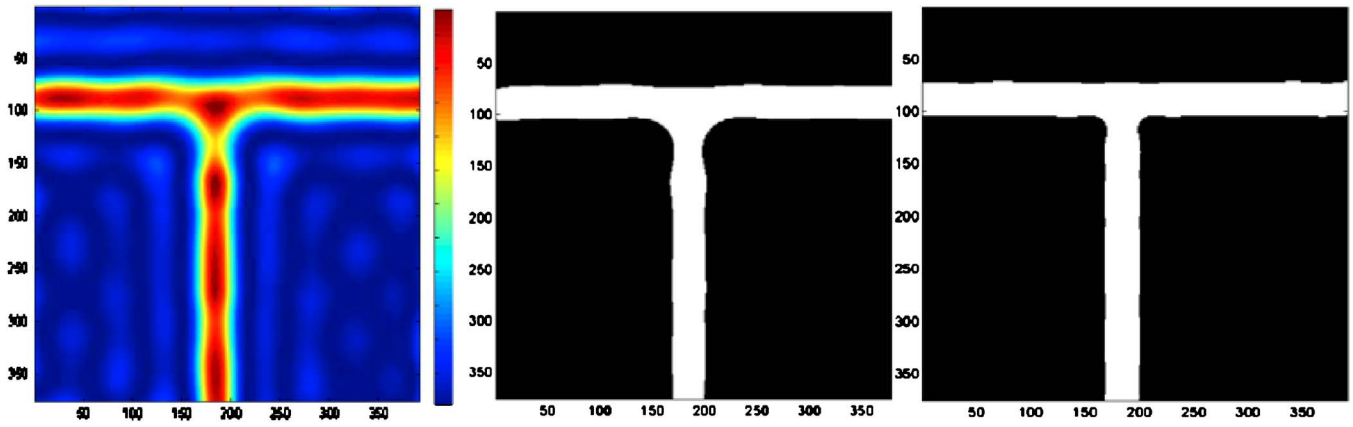

Fig. 5 The graph on the left is the aerial image obtained by solving the single-exposure ILT problem for the T junction. The center and right graphs are the contours at $t_r = 0.55$ (sampled at 2.5 nm) for single- and double-exposure ILT. The corresponding pattern errors are 1047 and 389.

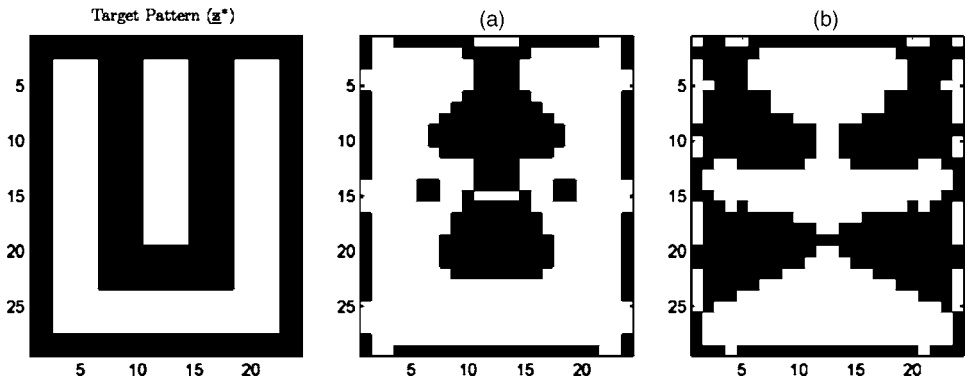

Fig. 6 The U-joint target pattern (left) and the two estimated chromeless PSM (center and right) obtained using method 2.

we have $\mathbf{a}^k=\mathbf{b}^k$. This is not helpful and against the spirit of double exposure, since the previous effect can be easily simulated with a single mask by merely doubling the dose. Hence, it is compulsory to initialize $\mathbf{a}$ and $\mathbf{b}$ at separate points for the success of this algorithm.

Furthermore, note that the optimization problem in Eq. (4) is subject to bound constraints given in Eq. (5). The prior can be reduced to an unconstrained optimization problem by using the parametric transformation $a_j=\sin(\omega_j)$ and $b_j=\sin(\psi_j)$ for $j=1,\ldots,MN$. The new parameter vector $\boldsymbol{\theta}=[\boldsymbol{\omega}^T,\boldsymbol{\psi}^T]^T\in\Re^{2MN\times 1}$, where $\boldsymbol{\omega}$ and $\boldsymbol{\psi}$ are the unconstrained vectors corresponding to $\mathbf{a}$ and $\mathbf{b}$ (see Ref. 7 for more details). The cost function defined in Eq. (4) is reformulated to obtain $F_1(\boldsymbol{\omega},\boldsymbol{\psi})$, and the gradient vectors $\mathbf{d}_1=\nabla_{\boldsymbol{\omega}}F_1(\boldsymbol{\omega},\boldsymbol{\psi})$ and $\mathbf{d}_2=\nabla_{\boldsymbol{\psi}}F_1(\boldsymbol{\omega},\boldsymbol{\psi})\in\Re^{MN\times 1}$ are evaluated. The steepest descent iterations are used to update both masks together as follows,

$$\boldsymbol{\theta}^{k+1}=\boldsymbol{\theta}^k-s\mathbf{d}^k, \tag{8}$$

where,

$$\mathbf{d}^k=\begin{bmatrix}\mathbf{d}_1^k\\ \mathbf{d}_2^k\end{bmatrix}.$$

Thus for every iteration, we move along the direction defined by the $2MN$ dimensional gradient vector $\mathbf{d}$, and *simultaneously* update both $\boldsymbol{\theta}_1$ and $\boldsymbol{\theta}_2$. The step size s is fixed by the user. The prior method works in practice, but its convergence is slow. In the next section, we explore a possible way of speeding up the convergence.

3.2 *Method 2: Cyclic Coordinate Descent*

We now introduce an alternative optimization strategy called cyclic coordinate descent. The latter involves optimizing the cost function with respect to only one parameter at a time, and sequentially covering up the whole parameter vector. Thus each coordinate axis (corresponding to a given parameter) is searched, and descent is made only along that particular dimension. The previous procedure is then repeated (cycling) until convergence is achieved. Thus at any point, we only make one dimensional moves along $a_1,\ldots,a_{MN},b_1,\ldots,b_{MN},a_1,\ldots$, in that order. However, we propose a slightly modified approach, which is in the spirt of the earlier schema. Instead of searching the $2MN$-dimensional space one dimension at a time, we split the search into *two MN* dimensional subspaces, corresponding to the two masks.

The procedure is as follows. We start by initializing the variables arbitrarily (usually $\mathbf{a}^0=\mathbf{b}^0=\mathbf{0}$) and do the parametric transformations (see Sec. 3.1) to obtain the uncon-

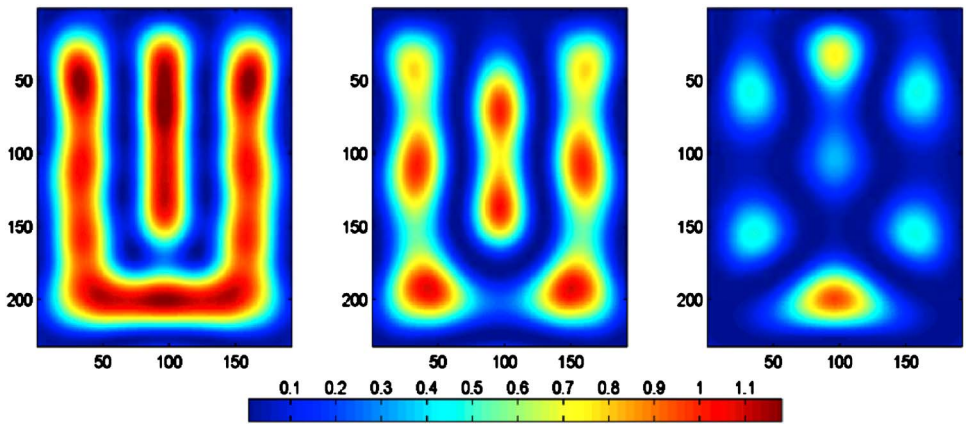

Fig. 7 The final aerial image (left) and the aerial images corresponding to the two individual exposures (center and right) for the mask patterns in Fig. 6.

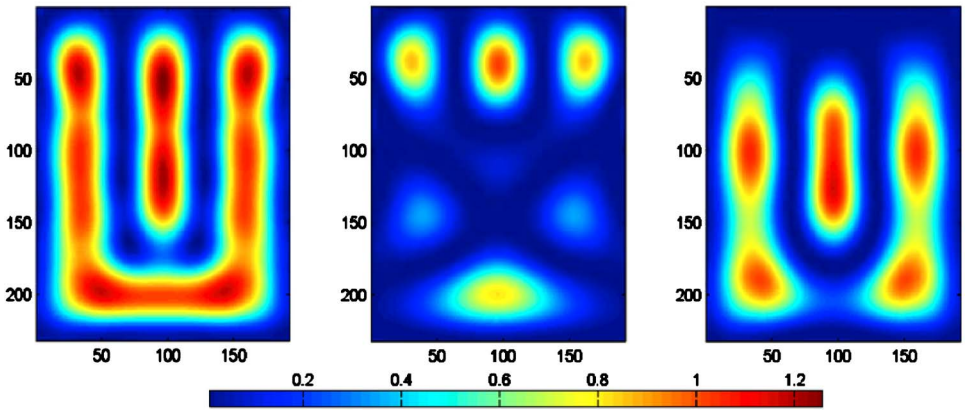

Fig. 8 The final aerial image (left) and the individual aerial images (center and right) for the U-joint target pattern. The corresponding masks were synthesized using method 1.

strained vectors $\boldsymbol{\omega}^0$ and $\boldsymbol{\psi}^0$. However, we update $\boldsymbol{\omega}$ and $\boldsymbol{\psi}$ separately on every iteration. Each iteration now consists of two steps. The first step involves updating only $\boldsymbol{\omega}$ by calculating the gradient of Eq. (4) with respect to $\boldsymbol{\omega}$. The second step involves updating only $\boldsymbol{\psi}$, but the gradient calculation utilizes the updated value of $\boldsymbol{\omega}$ (from the previous step). To summarize, for the k'th iteration,

$$\boldsymbol{\omega}^{k+1} = \boldsymbol{\omega}^k - s_1 \nabla_{\boldsymbol{\omega}} F_1(\boldsymbol{\omega}^k, \boldsymbol{\psi}^k), \tag{9}$$

$$\boldsymbol{\psi}^{k+1} = \boldsymbol{\psi}^k - s_2 \nabla_{\boldsymbol{\psi}} F_1(\boldsymbol{\omega}^{k+1}, \boldsymbol{\psi}^k). \tag{10}$$

At any point, we restrict our search only to the subspace defined by the other mask. Simulation results (see Sec. 4.3) indicate that method 2 has a faster convergence compared to method 1. It is also worth noting that the solutions obtained using methods 1 and 2 are not always equal, implying that there are multiple ways of splitting the patterns for double exposure (see Sec. 4.2 for more details).

4 Results

We now discuss some results obtained using the described framework. All the experiments were carried out for a 193-nm, fully coherent imaging system with $NA=0.85$ (unless stated otherwise).

4.1 *T Joint*

A T-joint suffers from the phase conflict problem. Hence direct rule-based phase assignments cannot be made, and special solutions have been proposed in the past to address this issue.[9,17] Figure 3 illustrates the desired pattern and the two synthesized chromeless phase-shift masks (PSMs) obtained using our double-exposure inverse lithography approach with method 2. The horizontal and vertical bars are 80 nm wide ($k_1=0.35$), and the mask pixel size is 20 nm in wafer dimensions (actual size 80 nm, assuming a 4× reduction factor). The aerial images in Fig. 4 illustrate that the first exposure prints the horizontal and vertical bars, but leaves a gap at their intersection. (The aerial images are up-sample by 8× using spline interpolation for display purpose.) This is the phase-conflict region. The second exposure deposits the missing energy in the previous region. The final aerial image has good contrast and is uniform along all portions (including the neck) with little visible rounding effect. Figure 5 illustrates the aerial image obtained using a chromeless PSM, which was synthesized by solving the *single-exposure* ILT problem. We observe that the aerial image in this case is weak (tending to break) near the junction, indicating a hot-spot. The L_2 normal cost function for single- and double-exposure cases was 39.81 and 35.12, respectively, indicating that the latter achieves a much better contrast. Figure 5 also indicates that the aerial image contours at $t_r=0.55$ have higher fidelity and much smaller *pattern error* for DEL-ILT. [Pattern error is defined as the total number of pixels not accurately reproduced in the binary output pattern. Note that the optimization was actually performed only for the aerial image and not the pattern fidelity. The pattern error can be further decreased using contour fidelity as the objective goal (see Ref. 18 for more details)]. Thus, DEL was able to resolve the phase conflict. Finally, the aerial image decomposition obtained

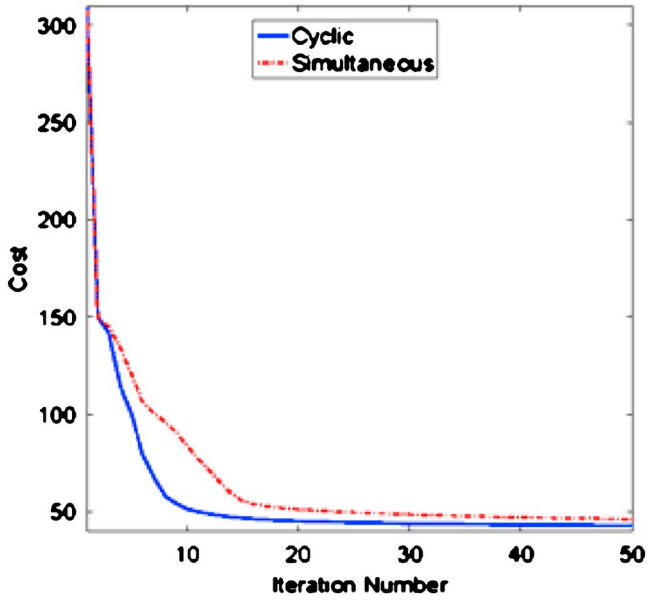

Fig. 9 Cost function behavior for simultaneous and cyclic descent algorithms when solving for the target pattern in Fig. 6.

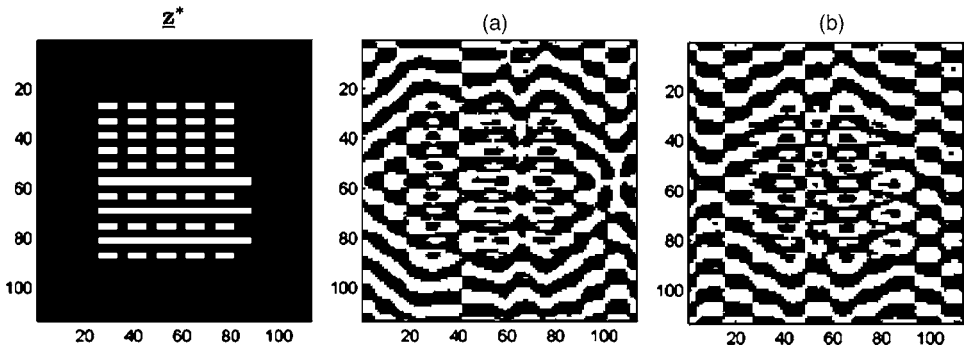

Fig. 10 The complex target pattern (left) and the two estimated chromeless PSM (center and right).

by employing method 1 is similar to the one seen in Fig. 4.

4.2 *U Joint*

Figure 6 illustrates the target pattern and the synthesized PSM for a vertical bar sandwiched between a U-shaped feature. The width of the features and their horizontal and vertical separations are 80 nm ($k_1=0.35$). The masks were synthesized using method 2 and 20-nm pixels similar to the previous case. The aerial images in Fig. 7 indicate a very interesting pattern decomposition. It appears that the algorithm is trying to split the original pattern into two sparser patterns, thereby increasing their effective critical dimensions and making them easier to print. The combined aerial image has a superior and uniform contrast compared to Fig. 1. The L_2 normal cost function of the aerial image is 40.09 (for DEL-ILT) versus 44.63 (for H-V decomposition approach in Fig. 1).

Figure 8 illustrates the aerial images obtained using the masks synthesized by method 1. The final cost function value is 40.49. We observe that the decomposition schema is different from that in Fig. 7. We believe that in general there may be multiple ways of splitting the target pattern for double exposure. The prior can be attributed to the ill-posedness of the inverse DEL problem. The *preferred* decomposition then depends on the regularization framework. For example, an interesting and important direction of future work is to find a decomposition schema that is highly tolerant to alignment errors.

The graph in Fig. 9 indicates the cost function behavior of the two algorithms (discussed in Sec. 3) for the first 50 iterations of the steepest descent algorithm. The rate of convergence depends on the chosen step size. To make a fair comparison, optimal step sizes were calculated on every iteration for both algorithms. The step sizes were calculated using the electrical caching technique discussed in Ref. 5. The double-exposure ILT problem was solved for the target pattern in Fig. 6. We observe that the cyclic descent method converges faster than the simultaneous descent method. This is true for all the target patterns discussed in this work. The computational complexity and number of convolutions required by the two algorithms is the same. Therefore, we conclude that the cyclic coordinate descent technique is a more superior way of searching the solution space.

4.3 *Verification Using Prolith*

We now want to verify our DEL-ILT aerial images using Prolith (a commercially available lithography simulation software from KLA-Tenor). Figure 10 illustrates a (complicated) target pattern and the synthesized CPL masks obtained using method 2. The target pattern was provided by Intel and consists of 60-nm features on a 120-nm pitch, the mask pixel size is 20 nm, $NA=0.93$, and $k_1=0.29$. The corresponding aerial images obtained using our forward model in Eq. (3) are given in Fig. 11. We observe that the algorithm attempts to alternately distribute the column of contacts between the two exposures. Thus it decomposes the

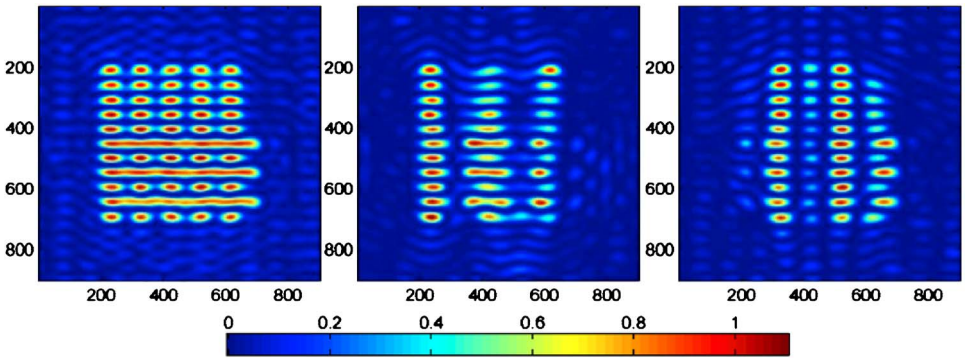

Fig. 11 The final aerial image (left) and the aerial images corresponding to the two individual exposures (center and right) for the mask patterns in Fig. 10.

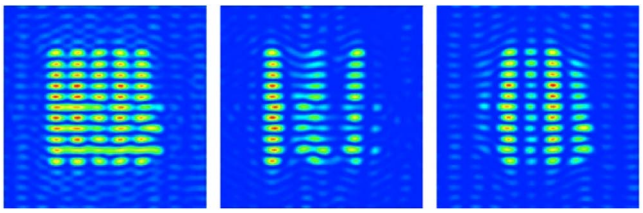

Fig. 12 The final aerial image (left) and the aerial images for the two individual exposures (center and right) obtained by feeding the mask patterns from Fig. 10 to Prolith.

original pattern into two comparatively sparser patterns, which can then be tackled separately during the individual exposures. The combined aerial image has a superior contrast, as observed in Fig. 11.

Figure 12 illustrates the aerial images obtained by feeding the ILT masks (in Fig. 10) to Prolith (provided by KLA-Tencor). The simulation was performed, assuming the Kirchhoff (thin-mask) approximation and using the same experimental settings as earlier. We observe that the results are in good overall agreement with those obtained in Fig. 11. The slight discrepancy in the results may be because we approximate an ideal low-pass filter using a finite extent spatial kernel, whereas Prolith calculates the aerial image directly in the frequency domain. We believe that the differences can be overcome if we employ the *exact* same forward model as Prolith.

5 Future Work and Conclusions

A framework for double-exposure inverse lithography mask synthesis is proposed. Initial solutions in the form of pixelated chromeless phase-shifted masks are demonstrated for typical patterns of interest using an idealized coherent imaging system and employing the Kirchhoff approximation. These suggest that the framework can indeed provide solutions for such a system with the contrast necessary to support patterning with optical lithography for future integrated circuit (IC) industry technology nodes.

While use of highly coherent illumination is indeed feasible in practice, and reformulation of the suggested framework for the case of partially coherent illumination can be done without significant negative impact to computational efficiency or loss of framework generality, use of the Kirchhoff approximation for forward imaging with subwavelength feature sizes will lead to large errors in the estimated exit electric field, and poor pattern fidelity. Therefore, any practical application of DEL-ILT will require the development of accurate and computationally efficient models to approximate the mask topography effects. This notwithstanding, the DEL-ILT solutions produced in this work follow the intuitive desire to decompose a pattern in a manner that increases the pitch, lowers the frequency content, and decreases the density, thereby making it easier to print using individual exposures. Perhaps most importantly, the algorithm is also automatically capable of resolving phase conflicts. It provides a new paradigm of splitting the (gray-level) aerial image into two parts, which we hope will point to a solution path that enables low k_1 double-exposure lithography over time.

DEL systems also need a critical alignment step in-between the two exposures, which has been neglected in the present discussion. Hence, an important direction of future work is to use the regularization framework to synthesize masks that are robust to alignment errors. There is also a need to explore smarter optimization algorithms like conjugate gradient or quasi Newton techniques, which can navigate the search space more effectively.

Acknowledgments

The authors would like to sincerely thank Yan Borodovsky from Intel for providing guidance on practical aspects of lithography. We would also like to thank KLA-Tencor for providing an evaluation license for Prolith, and Paul Davids from Intel for converting pixel-based masks to GDS-II. This work was supported by Intel Corporation.

References

1. S. Sayegh and B. Saleh, "Image design: generation of a prescribed image at the output of a bandlimited system," *IEEE Trans. Pattern Anal. Mach. Intell.* **5**, 441–445 (1983).
2. S. Sayegh, B. Saleh, and K. Nashold, "Image design: generation of a prescribed image through a diffraction limited system with high-contrast recording," *IEEE Trans. Acoust., Speech, Signal Process.* **33**, 460–465 (1985).
3. N. Cobb and D. Dudau, "Dense OPC and verification for 45 nm," *Proc. SPIE* **6154**, 61540I (2006).
4. Y. Liu, D. Abrams, L. Pang, and A. Moore, "Inverse lithography technology principles in practice: Unintuitive patterns," *Proc. SPIE* **5992**, 231–238 (2005).
5. Y. Granik, "Solving inverse problems of optical microlithography," *Proc. SPIE* **5754**, 506–526 (2005).
6. C. Hung, Q. Liu, K. Sakajiri, S. Shang, and Y. Granik, "Model based insertion of assist features using pixel inversion method: implementation in 65 nm node," *Proc. SPIE* **6283**, 62832y (2006).
7. A. Poonawala and P. Milanfar, "OPC and PSM design using inverse lithography: a nonlinear optimization approach," *Proc. SPIE* **6154**, 114–127 (2006).
8. M. Hasegawa, A. Suzuki, K. Saitoh, and M. Yoshii, "New approach for realizing k_1=0.3 optical lithography," *Proc. SPIE* **3748**, 278–287 (1999).
9. S. Hsu, J. Park, D. Van Den Broeke, and J. Chen, "Double exposure technique for 45 nm node and beyond," *Proc. SPIE* **5992**, 59921Q (2005).
10. M. Fritze, B. Tyrrell, D. Astolfi, R. Lambert, D. Yost, A. Forte, S. Cann, and B. Wheeler, "Subwavelength optical lithography with phase-shift-mask," *Lincoln Lab. J.* **14**, 237–250 (2003).
11. S. Zaidi and S. R. J. Brueck, "Multiple-exposure interferometric lithography," *Proc. SPIE* **2197**, 869–875 (1994).
12. X. Chen and S. R. K. Brueck, "Imaging intereferometric lithography for arbitrary patterns," *Proc. SPIE* **3331**, 214–224 (1998).
13. V. C. Pati and T. Kailath, "Phase-shifting masks for microlithography: Automated design and mask requirements," *J. Opt. Soc. Am. A Opt. Image Sci. Vis* **9**, 2438–2452 (1994).
14. Y. Wang, Y. Pati, H. Watanabe, and T. Kailath, "Automated design of halftoned double-exposure phase-shifting masks," *Proc. SPIE* **2440**, 290–301 (1995).
15. A. Poonawala and P. Milanfar, "Fast and low-complexity mask design in optical microlithography - an inverse imaging problem," *IEEE Trans. Image Process.* **16**, 774–788 (2007).
16. L. Pang, Y. Liu, and D. Abrams, "Inverse lithography technology (ILT), what is the impact on the photomask industry?," *Proc. SPIE* **6283**, 62830x (2006).
17. D. Bernard and J. Li, "Clear field dual alternating phase shift mask lithography," *Proc. SPIE* **4691**, 999–1008 (2002).
18. A. Poonawala, "Mask design for single and double exposure optical microlithography: an inverse imaging approach," PhD Dissertation, Univ. of California, Santa Cruz (2007).

Amyn Poonawala received the BE degree in Computer Engineering from the University of Mumbai, India, in 2001, and the MS and Ph.D. degrees in Computer Engineering from the University of California, Santa Cruz, in 2004 and 2007, respectively. His technical interests include inverse problems arising in single and double exposure optical microlithography. He is currently working as a R&D engineer at Synopsys Inc. where he is looking into practical aspects of inverse lithography.

Peyman Milanfar received the BS degree in electrical engineering and mathematics from the University of California, Berkeley, and the SM, EE, and PhD degrees in electrical engineering from the Massachusetts Institute of Technology, Cambridge, in 1988, 1990, 1992, and 1993, respectively. Until 1999, he was a senior research engineer at SRI International, Menlo Park, California. He is currently a professor of electrical engineering at University of California, Santa Cruz. He was a consulting assistant professor of computer science at Stanford University, California, from 1998 to 2000, where he was also a visiting associate professor in 2002. His technical interests are in statistical signal and image processing and inverse problems. He won a National Science Foundation Career award in 2000 and he was an associate editor for the *IEEE Signal Processing Letters* from 1998 to 2001. He is currently associate editor for IEEE Transactions on Image Processing.